Quasigeostrophic Dynamics of the Tropopause

MARTIN JUCKES

Department of Meteorology, University of Reading, Reading, United Kingdom

(Manuscript received 28 September 1993, in final form 23 February 1994)

ABSTRACT

The dynamical properties of potential temperature anomalies on the tropopause are analyzed for quasigeostrophic flow on an f plane. The potential vorticity is taken to be piecewise constant, with a single discontinuity at the tropopause. The tropopause potential temperature, on scales too small to feel the lower boundary, is found to be proportional to the tropopause geopotential height. The constant of proportionality is the geometric mean of the stratospheric and tropospheric lapse rates. Results from a general circulation model are found to be in agreement with this prediction.

The streamfunction associated with a combination of anomalies on the lower boundary and tropopause is also derived. The solution, determined completely by the potential temperature distributions, in general has a nonzero velocity at the lower boundary. Applying the theory to the time-mean zonal-mean jets, which must have a near-zero velocity at the ground, imposes a constraint on parameters defining the jet.

The dynamical properties of the system are further elucidated using the scaling argument previously applied by Charney to geostrophic turbulence. Charney's assumption of vertical homogeneity is replaced by the assumption that the dynamics is concentrated around the tropopause. In the nonlinear cascade to small scales the Rossby number is predicted to increase with horizontal wavenumber, leading to an eventual breakdown of geostrophic balance.

1. Introduction

Much of the dynamics of the troposphere is influenced by movement of the tropopause. This surface divides the well-mixed troposphere (low static stability, weak potential vorticity) from the stratosphere (high static stability, strong potential vorticity). In this paper the dynamics of the tropopause are examined for an idealized situation in which the potential vorticity is uniform in both the stratosphere and troposphere.

Potential vorticity and related concepts provide a useful means of decomposing and visualizing extratropical atmospheric flows (Hoskins et al. 1985). In quasigeostrophic theory the inversion operator relating velocity and height fields to the potential vorticity is linear. It follows that the flow contribution from different potential vorticity anomalies can be superimposed linearly to build up the total flow. This concept is used here to separate the flow associated with tropospheric and tropopause potential vorticity anomalies from that due to stratospheric anomalies. The piecewise constant form of the three-dimensional potential vorticity distribution considered here is conveniently represented in terms of the vertical displacement of the surface of discontinuity (the tropopause). The three-dimensional flow is thus specified by a two-dimensional field.

The restriction to quasigeostrophic flow excludes situations of great interest, such as tropopause folding. The results nevertheless give interesting insight into synoptic-scale dynamics.

Most work on the Eady model of baroclinic instability has used a rigid lid. This is equivalent to taking infinite static stability in the stratosphere. Previous work with finite stratospheric static stability has given analytic results only for linearized equations (e.g., Eady 1949; Pedlosky 1977; Garner et al. 1992). Rivest et al. (1992) analyze the properties of Eady baroclinic instability with a finite static stability in the stratosphere. Their normal modes have a structure consistent with that derived below for general tropopause potential temperature distributions. The derivation given below generalizes this aspect of their work by removing the dependence on linearization about an initial state.

A distinct issue, but closely related, concerns the extent to which a given velocity field can be attributed to the potential vorticity as opposed to the boundary conditions and variations in the background medium, such as variations in the static stability (Thorpe and Bishop 1993, personal communication).

The inversion calculations below are linear: this is because the nonlinearity of the equations does not enter into the inversion of the quasigeostrophic potential vorticity. No nonlinear terms have been neglected beyond the approximations made in the formulation of the quasigeostrophic equations. The restrictions on disturbance

Corresponding author address: Dr. Martin Juckes, Meteorologisches Institut der Universität München, Theresienstrasse 37, München 80333, Germany.

amplitudes necessary for linear time-dependent solutions are not needed here.

It is shown below that the dynamics of temperature anomalies on the tropopause is precisely equivalent to the dynamics of temperature anomalies on a solid surface, differing only by a rescaling of the timescale of the evolution by a factor that depends on the change in static stability across the tropopause. The properties of turbulence in such a system have been analyzed by Blumen (1978) and Hoyer and Sadourny (1982). Section 7 discusses their results and gives a simplified derivation of the spectral slope based on scale analysis.

2. Some preliminary GCM results

This work is to some extent motivated by the structure of the midlatitude troposphere in the U.K. Universities Global Atmospheric Modelling Project GCM (UGCM). This model is derived from a 1986 version of the European Centre for Medium-Range Weather Forecasts (ECMWF) forecast model; more details are given in Juckes et al. (1994). The model version used here includes a corrected radiation code (Li 1992) that reduces the noise in the temperature profiles and the consequent blurring of the tropopause that afflicted earlier experiments.

The tropopause can be defined either as a discontinuity in lapse rate or, following Reed (1955), as a discontinuity in potential vorticity (PV). In the idealized quasigeostrophic model discussed below the two definitions are equivalent. In the diagnostics of the numerical model the potential vorticity definition has been used. This definition is more closely linked with the theoretical ideas developed here. Previous observational work (e.g., Danielsen 1968) has suggested that the PV tropopause evolves more smoothly in time than that defined by the lapse rate. Hence, the former acts as a better indicator of the dynamical structure. In the GCM discussed here the lapse rate tropopause showed considerably more noise than the PV tropopause, but this may be in large part due to the use of a diagnostic algorithm that constrained the lapse rate tropopause to lie at one of the discrete model levels.

Figures 1 and 2 show longitude–pressure sections through the model. The shaded PV values mark the tropopause, separating regions with distinct PV characteristics (note that the contouring interval has been increased in the stratosphere to avoid saturation of the plot). In the stratosphere PV increases monotonically with height such that the isopleths form quasi-horizontal surfaces. In the troposphere, in contrast, the contours show a more complicated structure.

In both figures the tropopause has large vertical displacements associated with synoptic weather systems. The PV anomalies in the interior of the troposphere are weak compared with those associated with this displacement. This has the consequence that the dominant wind anomalies are those associated with the larger displacements of the tropopause. The dominance of the boundaries is further illustrated by the fact that none of the wind profiles shown has a maximum in the interior of the troposphere. The wind speed either increases monotonically from the lower boundary or has a minimum in the troposphere. It should be noted that if smaller scales were to be realistically represented these comments would probably not hold. Nevertheless, if we restrict attention to scales resolved by the model we can say that on those scales the wind field is consistent with PV anomalies concentrated at the boundaries of the troposphere. Note also in Figs. 1a and 2a that there is a strong negative correlation between the tropopause height and the height of upper-tropospheric potential temperature surfaces (heavy contours). This correlation is another illustration of the importance of the tropopause displacement.

3. The streamfunction associated with a tropopause temperature anomaly

It is natural to consider the tropopause as a material surface. This requires a slightly different approach to that used in standard quasigeostrophic theory. That theory linearizes the vertical advection of potential temperature (θ), so that

$$w\frac{\partial\theta}{\partial z} \approx w\frac{\partial\theta_0}{\partial z}. \tag{3.1}$$

This approximation is not strictly valid when the gradient of θ_0 is discontinuous because the neglected vertical gradient of perturbation potential temperature is in this case infinite. An alternative is to follow the vertical displacement (δz) of the tropopause explicitly. The approximation equivalent to Eq. (3.1) is then to linearize the equations with respect to δz. It is necessary to assume that δz is much smaller than the height scale of the flow: this is not a new restriction; it is equivalent to assuming small Rossby number [see scale analysis below Eq. (3.9)].

We take the tropopause to be a surface dividing two regions, the stratosphere and troposphere, with Brunt–Väisälä frequencies N_s and N_t. The potential vorticity is taken to be uniform in each region. The problem to be considered here is as follows: Given the potential temperature distribution on the tropopause, $\theta_{tp}(x, y)$, what is the associated geostrophic streamfunction and vertical displacement of the tropopause?

We will use the quasigeostrophic equations within each region and treat the tropopause as a material surface.

Since the potential vorticity is uniform in each region, the perturbation potential vorticity is zero. This gives

$$\frac{\partial^2\psi}{\partial x^2} + \frac{\partial^2\psi}{\partial y^2} + \frac{\partial}{\partial z}\left(\frac{f^2}{N_s^2}\frac{\partial\psi}{\partial z}\right) = 0 \tag{3.2}$$

in the stratosphere and a similar equation for the troposphere obtained by replacing N_s with N_t.

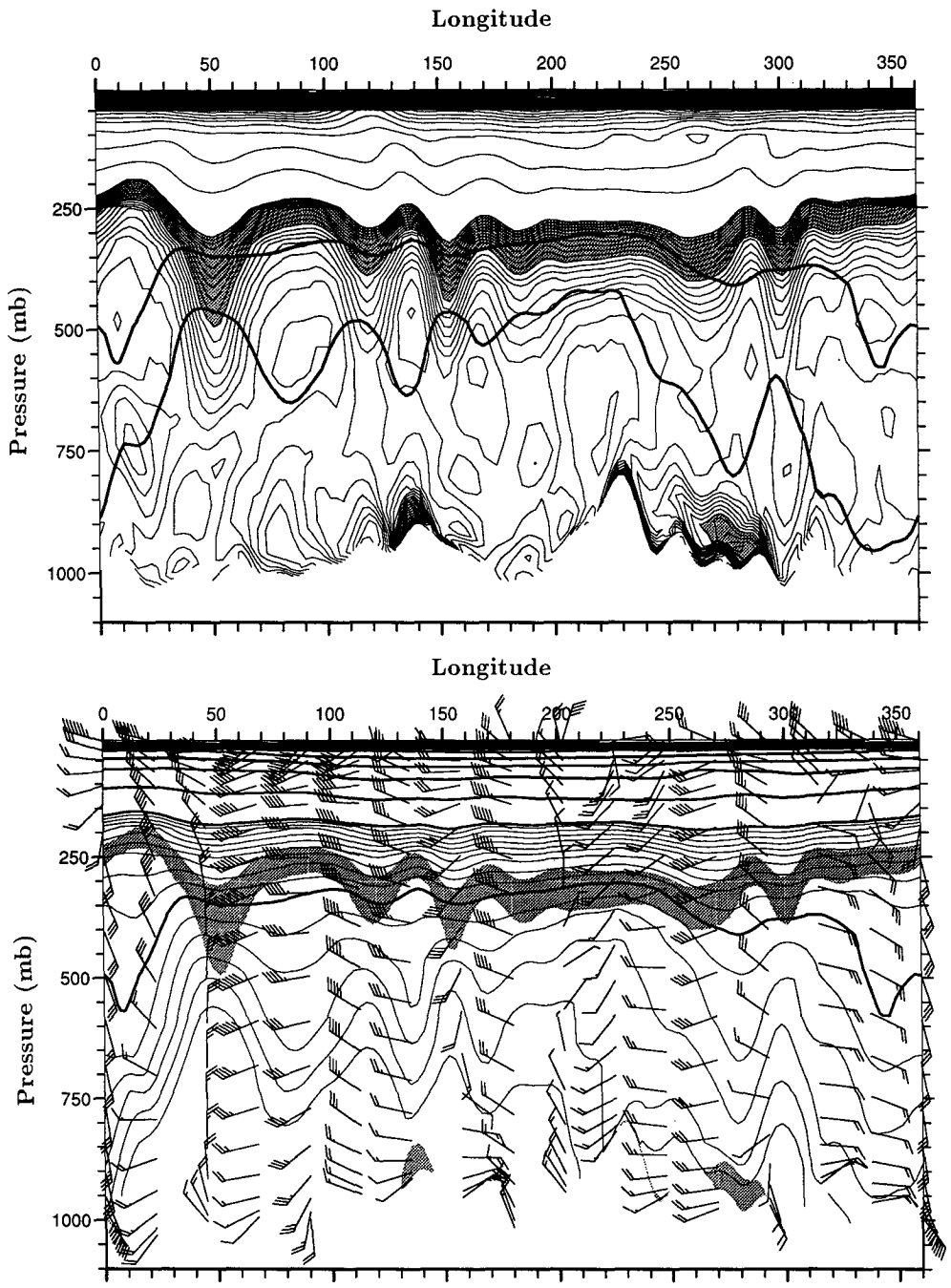

FIG. 1. Longitude–pressure sections from the UGCM at 60°N during December of a seasonal cycle experiment. (a) Ertel's potential vorticity (PV), shaded between 2 and 4, contour interval 0.2 (PV < 4) and 4 (PV > 4), where PV is in units of 10^{-6} K m^2 kg^{-1} s^{-1}. The two heavy contours show potential temperature of 285 and 300 K. (b) Potential temperature, contour interval 5 (below 350 K) and 50 (above 350 K). Wind barbs are shown for the horizontal wind, each flight corresponding to 5 m s^{-1}. The shading is the same as in (a).

In this section we neglect the lower boundary. This produces a simple result that is in remarkably good agreement with the behavior of the tropopause in a detailed numerical simulation (section 4). The boundary conditions used in this section are

$$\psi \to 0 \quad \text{as} \quad z \to \pm\infty \tag{3.3}$$

[as used by Rivest et al. (1992) in their analyses of linear Rossby waves on the tropopause] and ψ, θ continuous at the tropopause. The calculation including the

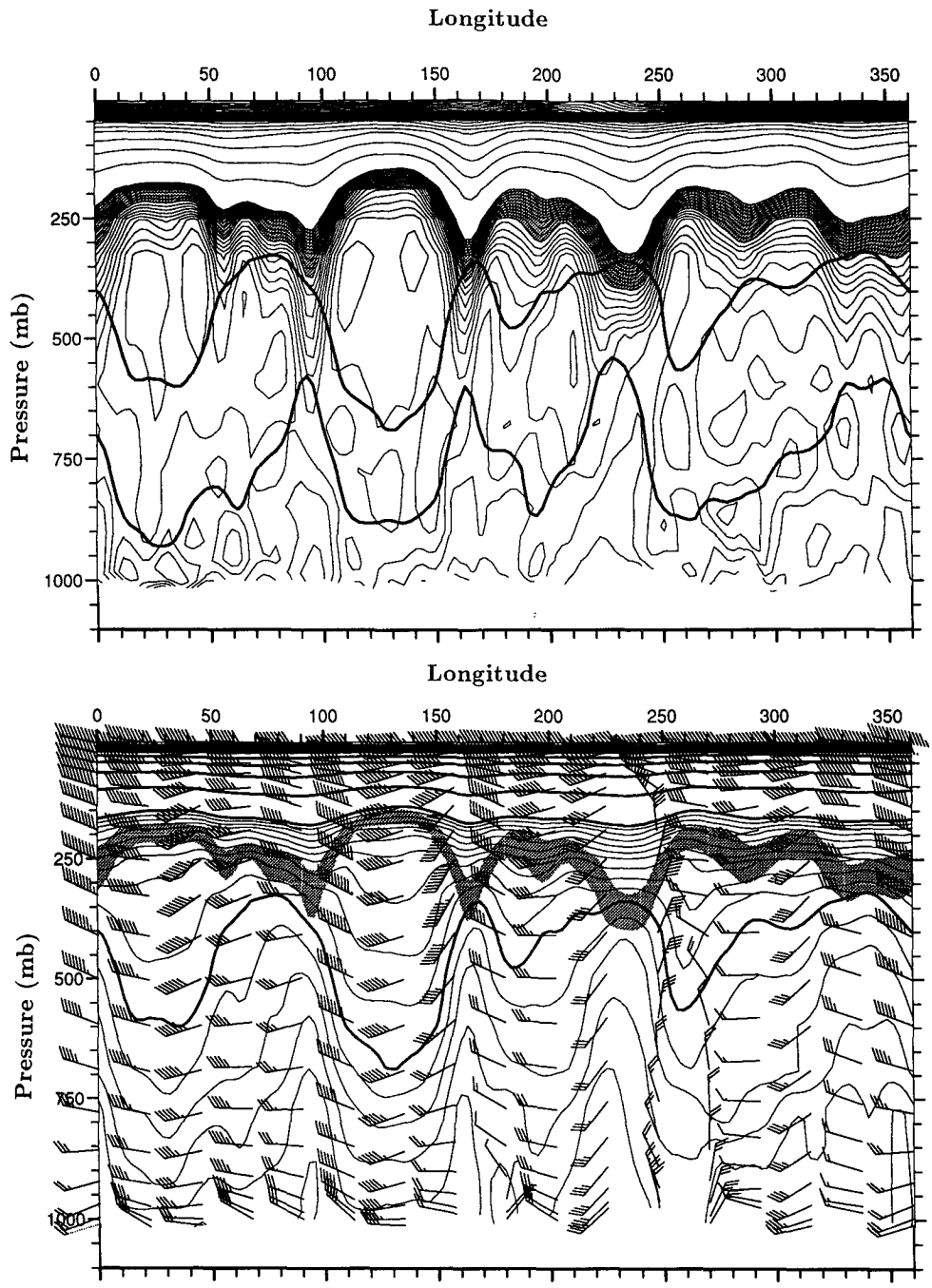

FIG. 2. As in Fig. 1 except at 50°S and the sign of potential vorticity is reversed.

lower boundary is given in section 5. The tropopause is displaced in the vertical by a distance δz from its undisturbed position at $z = 0$. The condition on θ here appears to be at odds with the usual condition that the vertical velocity (w) should be continuous. Continuity of w implies that θ' is discontinuous. The two approaches are consistent when allowance is made for the vertical displacement of the tropopause, as will be shown below.

Initially we consider a sinusoidal temperature perturbation

$$\theta'_{tp} = \tilde{\theta}_{tp}(\mathbf{k})e^{i\mathbf{k}\cdot\mathbf{x}}, \tag{3.4}$$

where $\mathbf{k}$ is a horizontal wave vector, $\mathbf{x} = (x, y)$ the horizontal position, and θ_{tp} is the potential temperature of the tropopause. The prime here and throughout the paper denotes a departure from a globally uniform basic state at rest. The perturbation includes any zonal-mean flow.

The boundary conditions at $z = \pm\infty$ together with continuity of ψ then imply solutions of the form

$$\psi = \begin{cases} Ae^{-(kN_s/f)z+i\mathbf{k}\cdot\mathbf{x}}, & z > 0, \\ Ae^{(kN_t/f)z+i\mathbf{k}\cdot\mathbf{x}}, & z < 0, \end{cases} \tag{3.5}$$

where $k = |\mathbf{k}|$ and A is a constant to be determined.

It is convenient to rescale ψ by defining

$$\psi^\dagger = \frac{\theta_{00} f}{g}\psi.$$

The potential temperature perturbation is given by

$$\theta' = \frac{\partial \psi^\dagger}{\partial z}. \tag{3.6}$$

Equations (3.5)–(6) then imply a relation between the potential temperature perturbation in the stratosphere $[\theta_s' = \theta'(0_+)]$ and troposphere $[\theta_t' = \theta'(0_-)]$:

$$N_t\theta_s' = -N_s\theta_t'. \tag{3.7}$$

The potential temperature anomalies in (3.7) show a change of sign across the tropopause. The total potential temperature, on the other hand, must remain continuous. These two properties are reconciled through the vertical displacement of the tropopause. At the displaced tropopause level there is a discontinuity between the basic-state profiles of the stratosphere and troposphere. These basic-state profiles are defined to have constant lapse rates and intersect at $z = 0$. Thus, $\theta_{0s}(z) = \theta_{0tp} + \Gamma_s z$ and $\theta_{0t}(z) = \theta_{0tp} + \Gamma_t z$ in the stratosphere and troposphere, respectively, where

$$\Gamma = \frac{d\theta_0}{dz} = \frac{\theta_{00}}{g}N^2$$

is the lapse rate. Hence, when the tropopause is displaced vertically the anomaly with respect to the tropospheric profile is no longer the same as that with respect to the stratospheric profile. The anomaly θ_{tp}' with respect to the potential temperature at the undisturbed position of the tropopause $[\theta_{0tp} = \theta_{0s}(0) = \theta_{0t}(0)]$ is related to the tropospheric and stratospheric perturbations as follows:

$$\begin{aligned} \theta_t' &= \theta_{tp}' - \delta z\Gamma_t, \\ \theta_s' &= \theta_{tp}' - \delta z\Gamma_s. \end{aligned} \tag{3.8}$$

Since $\Gamma_s > \Gamma_t > 0$ it follows that when δz is positive the stratospheric potential temperature anomaly θ_s' is less than the corresponding tropospheric anomaly θ_t'. Combining Eqs. (3.7) and (3.8) to eliminate θ_t' and θ_s' gives

$$\delta z = \frac{\theta_{tp}'}{\sqrt{\Gamma_t\Gamma_s}}. \tag{3.9}$$

This equation has been derived for a single wavenumber $\mathbf{k}$, but because $\mathbf{k}$ does not appear in Eq. (3.9) the result can trivially be summed over all wavenumbers and applied to an arbitrary temperature distribution.

The relationships between θ_t', θ_{tp}', θ_s', and δz are illustrated schematically in Fig. 3. The figure shows the undisturbed profile θ_0 (solid line) and a disturbed profile (dashed line). The dashed line is formed by adding anomalies that decay exponentially away from the tropopause and displacing the profile vertically. In this theory $\delta z(\partial\theta'/\partial z)$ is neglected [cf. neglect of $w(\partial\theta'/\partial z)$ in standard quasigeostrophic theory], so the perturbation temperatures can be evaluated at $z = 0$ or at $z = \delta z$. Simple scale analysis, assuming that the horizontal and vertical scales of the disturbance (L_x and L_z, respectively) are related by $L_z/L_x = f/N$ and that the temperature and velocity perturbations scale in accordance with the gradient wind relation, yields $\delta z/L_z = O(U/fL_x)$, where U is the velocity scale. This means that the linearization with respect to δz is valid whenever quasigeostrophic theory is valid. In the figure, δz has been exaggerated to illustrate the exponential nature of the disturbed profiles.

Using (3.5), (3.6), (3.8), and (3.9) we can derive the amplitude of the streamfunction

$$A = \frac{\tilde{\theta}_{tp} g(N_s - N_t)}{\theta_{00} k N_s N_t}. \tag{3.10}$$

The relationships expressed in Eqs. (3.9) and (3.10) are found in the edgewave solutions calculated by Rivest et al. (1992) for linear disturbances on the tropopause [there is, however, a minor error in the relevant equation, bottom of p. 2113, of their paper: their previous equations imply, as here, $\delta z = Ak/(N_s - N_t)$. This error does not affect the conclusions of their paper]. Unlike their calculation the present result, though more limited in other respects, does not rely on linearization of the quasigeostrophic equations.

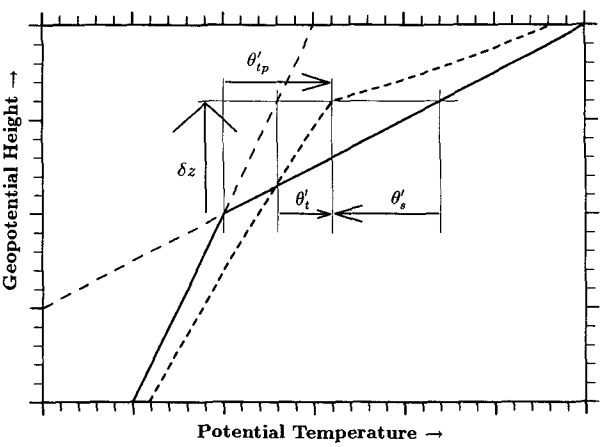

FIG. 3. Schematic plot of potential temperature against height illustrating the displacement of the profile, which accompanies a potential temperature anomaly at the tropopause. Plotted are the undisturbed profile (solid) and the perturbed profile (short dashes). See text for discussion.

Following Bretherton (1966), the potential temperature distribution can be expressed as an equivalent potential vorticity distribution,

$$q = -f\left(\frac{N_s^2 - N_t^2}{N_s^2 N_t^2}\right)\frac{g\theta'_{tp}}{\theta_{00}}\,\delta(z). \qquad (3.11)$$

Equation (3.11) can be used to estimate the strength of tropopause θ anomalies relative to tropospheric PV anomalies. The typical magnitude of θ'_{tp} in the UGCM is 10 K, slightly larger in the Southern Hemisphere (Fig. 2) than in the Northern Hemisphere (Fig. 1). Taking $N_s^2 = 4N_t^2 = 4 \times 10^{-4}\ \mathrm{s}^{-2}$, $g = 10\ \mathrm{m\ s}^{-2}$, and $\theta_{00} = 300$ K in Eq. (3.11) and integrating vertically across the tropopause gives $\int q dz = 2.5f$ km. The anomalies in Ertel's potential vorticity shown in Figs. 1 and 2, with values ≈ 0.4 in the troposphere, can be related to anomalies in quasigeostrophic potential vorticity through $q \approx g^{-1}\mathrm{PV}\ dp/d\theta_0$. Taking $dp/d\theta_0 = 25$ mb K^{-1} and an anomaly depth of 5 km gives a strength of $\approx 0.5f$ km. This implies that the neglect of tropospheric potential vorticity will give an error of the order of 20%, the error being slightly smaller in the Southern Hemisphere. These figures are only presented here to give a crude estimate of the approximations made in the theory; other months and latitudes may give slightly different answers.

4. Comparison with data and GCM results

The local relation between the height and temperature of the tropopause is an attractively simple result and provides a good basis to test the applicability of the above theory to real data or GCM results. This is a test of the hypothesis that the PV anomalies within the troposphere are, in some sense, less important than those associated with perturbations of the tropopause. A caveat is needed because the smallness of one measure of the influence of internal PV anomalies does not necessarily imply that their influence on the evolution of the flow is small (cf. the ageostrophic velocity field, which plays an essential role in the development of weather systems despite being considerably smaller than the geostrophic velocity).

The relationship given in Eq. (3.9) may appear to be an obvious consequence of the general increase of θ with height in the atmosphere. A high tropopause is generally warm, as seen from observations, but the question is why. A simple thought experiment shows that it need not always be the case. Suppose we start with a flow at rest, so that the tropopause has uniform potential temperature. If potential vorticity anomalies are created in the troposphere, then corresponding wind and height anomalies will appear at the tropopause. In the absence of local diabatic forcing, however, the potential temperature of the tropopause remains unchanged. Thus, for a general potential vorticity distribution, the height and potential temperature of the tropopause are not necessarily correlated.

The idealized model discussed in the previous section has a discontinuity in potential vorticity. In the GCM the tropopause is less well defined. Following Hoskins et al. (1985), the PV $= \pm 2$ surface is used here, where PV is in units of $10^{-6}\ \mathrm{Km^2\ kg^{-1}\ s^{-1}}$. Figure 4 shows the potential temperature and height of this surface in the UGCM. The two fields show many common features. Between 20° and 40°S they are in close agreement. At these latitudes the smallness of f and the relatively high tropopause both tend to reduce the contribution to δz from temperature anomalies at the ground. A similar high correlation between height and potential temperature of the PV $= 2$ surface is seen in analyses from the U.K. Meteorological Office forecast system (T. Hewson 1993, personal communication).

Figure 5 shows a scatterplot made from 42 days of data on the same surface between 15° and 60°S, sampled at 6-day intervals. The quantity contoured is the number of grid points falling in a 1 K by 1 km box. Figure 5a is constructed from the total fields, and Fig. 5b from the eddy components. Both show a linear relationship. The above theory applies in principle to both the eddy and the zonal-mean components of the flow, but the neglect of the lower boundary condition will be inaccurate for large scales. In Fig. 5b the zonal mean has been removed to get rid of the largest scales. The resulting slope is about 6 K km^{-1}, consistent with Eq. (3.9) when the lapse rates are given values of $\Gamma_t = 3$ K km^{-1} and $\Gamma_s = 12$ K km^{-1}. When the zonal mean is included (Fig. 5a) the slope is slightly different, about 9 K km^{-1}. This difference must be due in part to the influence of the lower boundary. The effect of the lower boundary is studied in the following two sections.

Of course, interactions between the tropopause and the lower boundary play a fundamental role in the dynamics of the storm tracks, leading to the conversion of potential to kinetic energy. This process is often modeled through linear normal-mode calculations, although Farrell (1984) has shown that other mechanisms may also be important in reality. For mathematical simplicity we consider here the Eady mode of linear instability, as discussed by Rivest et al. (1992). As mentioned in the introduction, they consider normal modes on a linear shear with a discontinuity of static stability at the tropopause. The ratio of θ_{tp} to δz is then a complex function of wavenumber and the ratio of static stabilities. If we take, for simplicity, $N_s = 2N_t$ and the wavenumber of the fastest-growing mode (in a channel of width 2000 km), then their results give $\theta_{tp} = \delta z \times (5.7 + 1.0i)$ K km^{-1}, compared with $\delta z \times 6$ K km^{-1} derived above. This diagnostic does not, therefore, distinguish clearly between linear interactions between the tropopause and ground on the one hand and nonlinear dynamics of the tropopause on the other hand. Both theories depend on the neglect of potential vorticity anomalies within the troposphere.

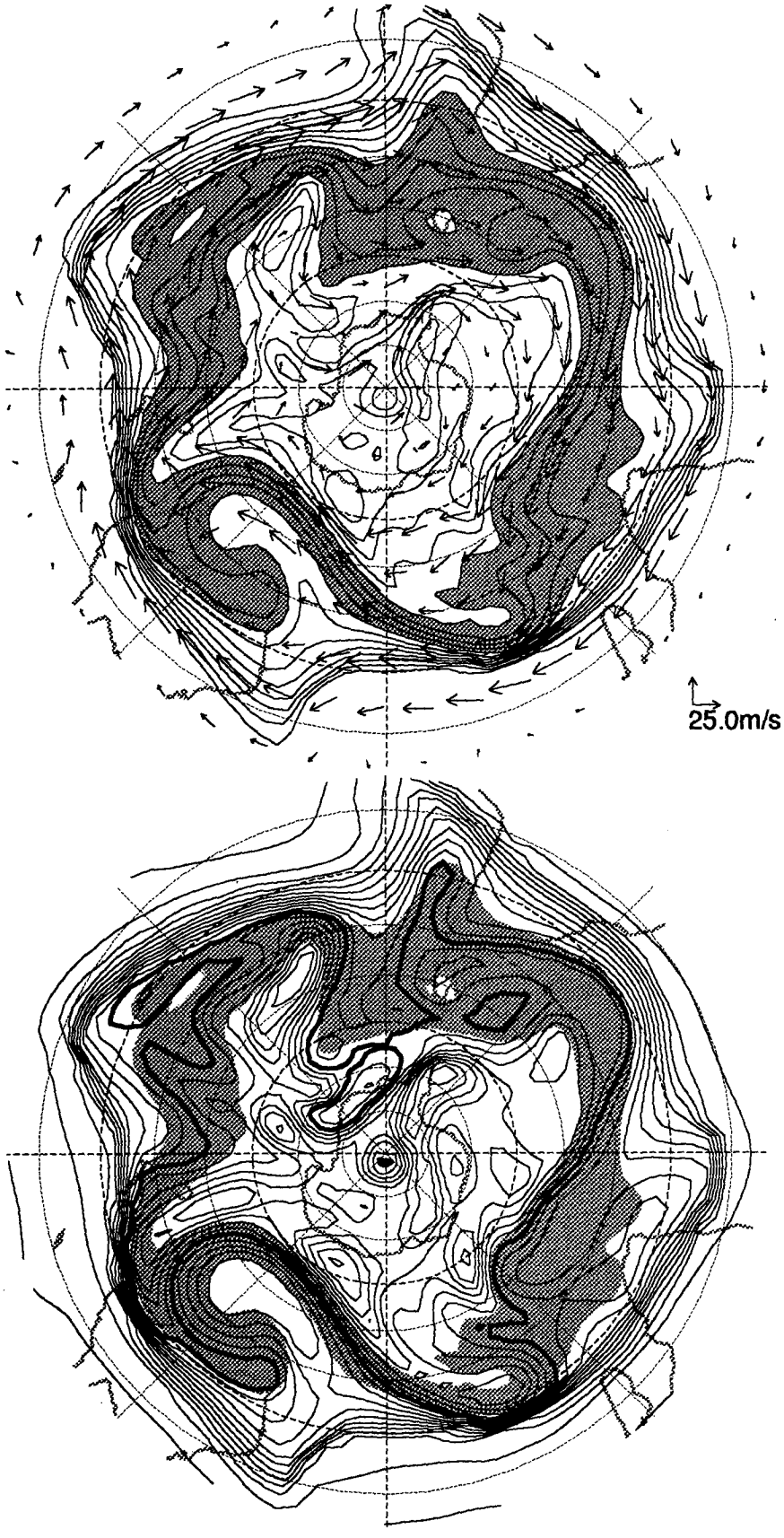

FIG. 4. (a) Potential temperature (contour interval 5 K, shaded between 310 and 330 K) and winds on the PV = −2 surface. Polar stereographic projection, outer limit 15°S. The Greenwich meridian is to the right. (b) Geopotential height of the PV = −2 surface (contour interval 500 m; heavy contour is 10 000 m). The shading is the same as in (a).

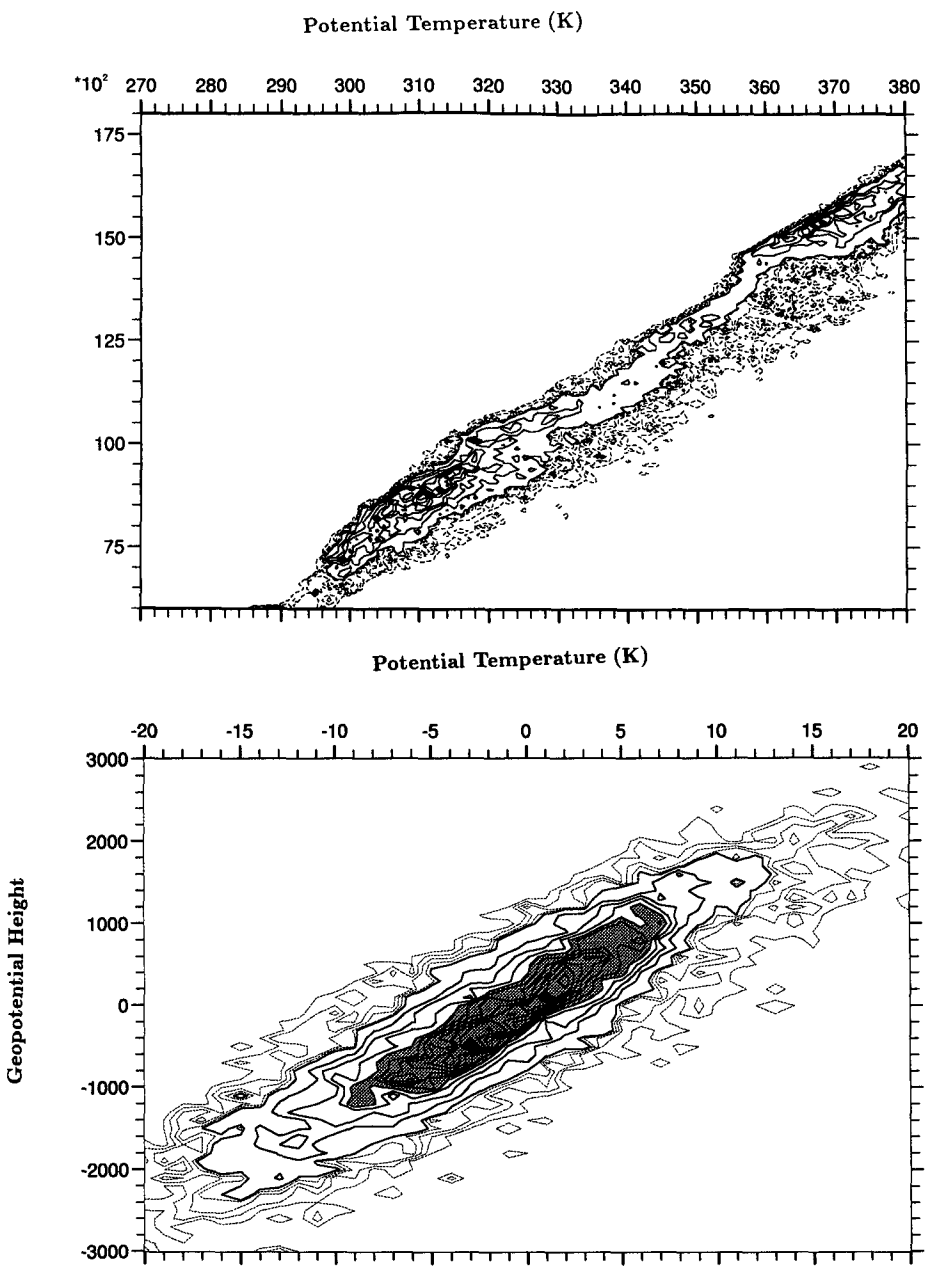

FIG. 5. Contoured scatterplot of potential temperature versus geopotential height on the PV = −2 surface, between 15° and 60°S. The data are taken from the start of June through to mid-July at 6-day intervals. (a) Total fields and (b) departures from the zonal mean. In both cases the number of points falling in a 1 K × 1 km box is contoured; contour interval 10 (solid) and 2 (dashed, up to 8).

5. Streamfunction associated with temperature anomalies on both tropopause and lower boundary

On larger scales the tropopause cannot be treated in isolation. Temperature anomalies at the ground must also be taken into account. We also include here the density stratification and potential temperature scale height (e.g., Bannon 1989). The potential vorticity anomaly is now

$$q = \nabla_h^2 \psi + \rho_0^{-1} \frac{\partial}{\partial z} \frac{\rho_0 f^2}{N^2} \frac{\partial \psi}{\partial z} = 0, \qquad (5.1)$$

where $\rho_0 = \rho_{00} \exp(-z/H_\rho)$. The potential temperature is related to the streamfunction by

$$\frac{\partial \psi^\dagger}{\partial z} - \frac{\psi^\dagger}{H_\theta} = \theta'. \qquad (5.2)$$

We will take the density scale height H_ρ to be uniform

and the potential temperature scale height to have distinct values, $H_{\theta s}$ and $H_{\theta t}$, in the stratosphere and troposphere, respectively. Instead of $\psi^\dagger \to 0$ as $z \to -\infty$ the lower boundary condition becomes

$$\frac{\partial \psi^\dagger}{\partial z} - \frac{\psi^\dagger}{H_\theta} = \theta_g', \quad z = -H, \tag{5.3}$$

where H is the depth of the troposphere and the subscript g stands for ground.

The solution now takes the following form:

$$\psi^\dagger = \begin{cases} Ae^{m_s^- z + i\mathbf{k}\cdot\mathbf{x}}, & z > 0 \\ [Be^{m_t^- z} + Ce^{m_t^+ z}]e^{i\mathbf{k}\cdot\mathbf{x}}, & z < 0, \end{cases} \tag{5.4}$$

where

$$m_{s/t}^{\pm} = \frac{1}{2H_\rho} \pm \left(\frac{1}{4H_\rho^2} + \frac{N_{s/t}^2 k^2}{f^2}\right)^{1/2}. \tag{5.5}$$

Applying the boundary conditions leads to the relations

$$A = B + C, \tag{5.6}$$

$$(m_s^- - H_{\theta s}^{-1})A = \tilde{\theta}_{tp} - \tilde{\delta z}\Gamma_s, \tag{5.7}$$

$$(m_t^- - H_{\theta t}^{-1})B + (m_t^+ - H_{\theta t}^{-1})C = \tilde{\theta}_{tp} - \tilde{\delta z}\Gamma_t, \tag{5.8}$$

$$(m_t^- - H_{\theta t}^{-1})Be^{-m_t^- H} + (m_t^+ - H_{\theta t}^{-1})Ce^{-m_t^+ H} = \tilde{\theta}_g, \tag{5.9}$$

where the tilde denotes a Fourier coefficient, as in Eq. (3.4). These equations define the four unknowns, A, B, C, and $\tilde{\delta}z$, as functions of ground and tropopause potential temperature anomalies.

For convenience we define $a = (m_s^- - H_{\theta s}^{-1})$, $b = (m_t^- - H_{\theta t}^{-1})$, and $c = (m_t^+ - H_{\theta t}^{-1})$. The solution is

$$LA = -\tilde{\theta}_{tp}(\Gamma_s - \Gamma_t)(ce^{-m_t^+ H} - be^{-m_t^- H}) + \tilde{\theta}_g\Gamma_s(c - b), \tag{5.10}$$

$$LB = -\tilde{\theta}_{tp}(\Gamma_s - \Gamma_t)ce^{-m_t^+ H} + \tilde{\theta}_g(c\Gamma_s - a\Gamma_t), \tag{5.11}$$

$$LC = \tilde{\theta}_{tp}(\Gamma_s - \Gamma_t)be^{-m_t^- H} - \tilde{\theta}_g(b\Gamma_s - a\Gamma_t), \tag{5.12}$$

$$L\delta z = \tilde{\theta}_{tp}(b(c - a)e^{-m_t^- H} - c(b - a)e^{-m_t^+ H}) + \tilde{\theta}_g a(b - c), \tag{5.13}$$

where $L = (a\Gamma_t - b\Gamma_s)ce^{-m_t^+ H} - (a\Gamma_t - c\Gamma_s) \times be^{-m_t^- H}$.

Figure 6 shows the sensitivity of δz to variations in $\tilde{\theta}_{tp}$ and $-\tilde{\theta}_g$ as a function of horizontal scale L_y with all other parameters in Eq. (5.13) held constant at the values given in Eq. (6.6). As expected, the link between δz and θ_g is weak at small scales and increasingly strong at larger scales. The larger-scale flow includes the zonal-mean jets. The constraints expressed by (5.10)–(13) provide some information about the zonal-mean jet structure, insofar as that structure is geostrophic and dominated by the tropopause. This topic is investigated further in the next section.

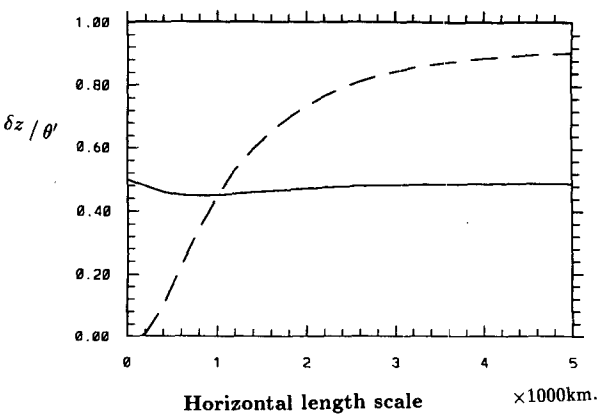

FIG. 6. Coefficients from Eq. (5.13), normalized by the tropospheric lapse rate, showing sensitivity of tropopause height (δz) to variations in θ_{tp}' (solid line) and $-\theta_g'$ (dashed line) as a function of horizontal scale; that is, $\Gamma_t L^{-1}[b(c - a)e^{-m_t^- H} - c(b - a)e^{-m_t^+ H}]$ and $-\Gamma_t L^{-1}a(b - c)$, respectively.

6. Zonal-mean jets

This section uses the above result as a basis for some qualitative remarks concerning the time-mean flow of the troposphere. The results of the previous section were derived for an f plane, so they are only strictly valid for scales much less than the planetary scale. Nevertheless, much work has been done using the f-plane approximation to study larger scales in a qualitative manner; the same approach is adopted here.

The large-scale time-mean wind at the lower boundary is constrained by friction to be near zero. Using Eqs. (5.11) and (5.12), the streamfunction at the lower boundary is given by

$$\begin{aligned}\psi_g^\dagger &= [Be^{-m_t^- H} + Ce^{-m_t^+ H}]e^{i\mathbf{k}\cdot\mathbf{x}} \\ &= L^{-1}[\tilde{\theta}_{tp}(\Gamma_s - \Gamma_t)(b - c)e^{-H/H_\rho} \\ &\quad + \tilde{\theta}_g(a\Gamma_t(e^{-m_t^+ H} - e^{-m_t^- H}) \\ &\quad + \Gamma_s(ce^{-m_t^- H} - be^{-m_t^+ H}))]e^{i\mathbf{k}\cdot\mathbf{x}}. \end{aligned} \tag{6.1}$$

Setting $\psi_g^\dagger = 0$ gives an identity relating $\tilde{\theta}_{tp}$ and $\tilde{\theta}_g$. Since the wind is not precisely zero at the ground $\psi_g^\dagger$ is retained as a parameter. Rearranging (6.1) gives

$$F = \frac{\tilde{\theta}_g[a\Gamma_t(e^{-m_t^+ H} - e^{-m_t^- H}) + \Gamma_s(ce^{-m_t^- H} - be^{-m_t^+ H})] - \tilde{\psi}_g^\dagger L}{\tilde{\theta}_{tp}(\Gamma_s - \Gamma_t)(c - b)e^{-H/H_\rho}} = 1. \tag{6.2}$$

The constraint on the wind at the ground applies to the zonal-mean flow, so the horizontal wavenumber k must now be interpreted as representative of the meridional wavenumber of the zonal-mean flow. The constraint can be considered as a parametrization of the effects of baroclinic eddies because it is a consequence of the uniformity of tropospheric PV, which in turn results from mixing associated with baroclinic eddies.

Here H and Γ_t appear as independent parameters, but this is not necessarily the most appropriate approach.

Let the mean temperature at the ground be θ_{0g} and the stratospheric profile be $\theta_{0s}(z) = \theta_{rs} + \Gamma_s(z + H)$, where θ_{rs} is a constant. Continuity of the basic state at the tropopause implies

$$\theta_{0g} + \Gamma_t H = \theta_{rs} + \Gamma_s H. \tag{6.3}$$

Following Held (1982) θ_{0g}, θ_{rs}, and Γ_s can be considered as radiatively determined, while the dynamics of the troposphere determines Γ_t and H (through diabatic processes associated with baroclinic waves). From this point of view the latter two variables are not independent. Using (6.3) Γ_t can be eliminated from (6.2), so that we have

$$F = F(H, L_y, \theta_{0g}, \theta_{rs}, \Gamma_s, \tilde{\theta}_g, \tilde{\theta}_{tp}, H_{\theta t}, H_{\theta s}, H_\rho, \tilde{\psi}_g^\dagger) = 1. \tag{6.4}$$

If ten parameters are specified, the remaining parameter can be predicted by Eq. (6.4). For instance, taking

$$(H, L_y, \theta_{0g}, \theta_{rs}, \Gamma_s, \tilde{\theta}_g, \tilde{\theta}_{tp}, H_{\theta p}, H_{\theta s}, H_\rho, \psi_g^\dagger) = (10\text{ km}, 3000\text{ km}, 280\text{ K}, 190\text{ K}, 12\text{ K km}^{-1}, 30\text{ K}, \tilde{\theta}_{tp}, 8\text{ km}, 100\text{ km}, 28\text{ km}, 0), \tag{6.5}$$

for which values the corresponding tropospheric lapse rate, from Eq. (6.3), is $\Gamma_t = 3$ K km^{-1}, gives a prediction $\tilde{\theta}_{tp} = 150$ K and $\tilde{\delta z} = 16$ km. These predictions are somewhat larger than observed. In the UGCM, for instance, the variation in tropopause temperature between 30° and 60°S is of the order of 60 K and the variation in height is around 7 km. A decrease in Γ_t, which might be considered an effect of moisture, reduces the predictions but is not sufficient to account for the discrepancy. For instance, setting $\theta_{rs} = 160$ K (and hence $\Gamma_t = 0$) gives $\tilde{\theta}_{tp} = 100$ K and $\delta z = 12$ km.

The choice of L_y used above is equivalent to a half wavelength of 90° latitude. Because the theory uses the f plane it is not possible to make a uniquely well defined identification between L_y and atmospheric parameters. The predicted values of $\tilde{\theta}_{tp}$ and $\tilde{\delta z}$ are sensitive to the choice of L_y (δz is the most sensitive, taking values 18 and 15 km at $L_y = 2000$ and 4000 km, respectively), so, not surprisingly, the theory has little predictive power. On the other hand, the underlying dynamics that lead to Eq. (6.4) do resemble those of the atmosphere, so it is likely that a similar constraint will remain when a more realistic model is used.

Since F is a constant, any change in one of the above parameters must be balanced by changes in the others so as to maintain that constant value. Thus,

$$\sum_{i=1,10} \frac{\partial F}{\partial \ln p_i} \frac{\Delta p_i}{p_i} + \frac{\partial F}{\partial \psi_g^\dagger} \Delta\psi_g^\dagger = 0, \tag{6.6}$$

where $\{p_i : i = 1, 10\}$ are the first ten arguments in (6.4). The logarithmic derivatives of these 10 evaluated at the parameter values given above [Eq. (6.5)] are

$$(2.7, -0.1, -4.3, 2.9, 1.4, 1.0, -1.0, 0.05, -0.05, -1.2), \tag{6.7}$$

and the derivative with respect to $\psi_g^\dagger$ normalized by the tropopause streamfunction is

$$\frac{\partial F}{\partial \psi_g^\dagger} \psi_{tp}^\dagger = 0.4. \tag{6.8}$$

For expected climate changes the changes in density and potential temperature scale heights can be neglected. Changes in θ_{0g} and θ_{rs} are likely to be of the order of 1%, so can be neglected relative to changes in $\tilde{\theta}_g$. In the context of CO_2-induced warming, changes in Γ_s are also expected to be small. The remaining five parameters are then related by

$$\frac{\Delta\tilde{\theta}_g}{\tilde{\theta}_g} - \frac{\Delta\tilde{\theta}_{tp}}{\tilde{\theta}_{tp}} + 2.7\frac{\Delta H}{H} - 0.1\frac{\Delta L_y}{L_y} + 0.4\frac{\Delta\psi_g^\dagger}{\psi_{tp}^\dagger} \approx 0. \tag{6.9}$$

Since $\psi_g^\dagger/\psi_{tp}^\dagger$ is small (≈ 0.1 for a realistic zonal flow) the last term is likely to be small.

Equation (6.9) constrains the way in which the mean tropopause height (H) and the slope [$\tilde{\delta z}$, related to $\tilde{\theta}_{tp}$ and $\tilde{\theta}_g$ through Eq. (5.13)] can change in response to a change in pole to equator temperature gradients.

These equations give a diagnostic link between the parameters, but do not establish any causal link. If, for instance, the static stability of the troposphere N_t is determined by the moist-adiabatic lapse rate or by details of baroclinic instability (Held 1982), then the variations in tropopause height (δz) and $\tilde{\theta}_s$ are predicted as functions of the lower boundary temperature gradient $\tilde{\theta}_g$. If, on the other hand, the stratospheric radiation balance constrains $\tilde{\theta}_s$ in some way, then N_t is given as a function of $\tilde{\theta}_g$.

It should be noted, however, that $\tilde{\theta}$ here is the temperature field associated with ground and tropopause temperature anomalies. At the ground this might be a reasonable approximation to the total flow, but the same is not true in the stratosphere. The total temperature field in the stratosphere will contain large contributions from local PV anomalies. Thus, $\tilde{\theta}_s$ represents only one component of the stratospheric field, so it is not easy to estimate how it will vary in different climate scenarios.

Most studies of the Eady model use a basic state with no meridional variation, corresponding to $k = 0$ in the results of this section, and also neglect effects of the density and potential temperature scale heights. The structure of the streamfunction in the limit $k \to 0$ is then linear in the troposphere and constant in the stratosphere. This limit is singular in that the upper boundary condition, $\psi \to 0$ as $z \to \infty$, is no longer satisfied. A slightly weaker form of the boundary condition, that ψ

remains bounded, is satisfied. In this limit F becomes independent of H and the upper boundary condition on ψ can only be satisfied if $\theta_s' = 0$.

7. Nonlinear dynamics

The storm tracks in the atmosphere are characterized by strongly nonlinear dynamics. Some general properties of the flow can be deduced from scaling arguments and the global conservation properties of the dynamical system. This approach depends on an assumption that the dynamics over a significant range of scales is independent of any externally imposed length scales. Charney (1971) used such methods to analyze the properties of quasigeostrophic turbulence with a three-dimensionally isotropic (with rescaled vertical coordinate) and homogeneous streamfunction. In spite of the neglect of both the lower boundary and the strong vertical inhomogeneity associated with the tropopause, Charney's analysis does capture important features of the large-scale nonlinear dynamics (e.g., Boer and Shepherd 1983). The ideas developed in the previous sections suggest an alternative idealization—namely, horizontally homogeneous turbulence confined to a vertical discontinuity in the static stability.

We consider here the system analyzed in section 3, neglecting the ground. Setting $\theta^* = (1 - N_t/N_s)\theta_{tp}$, the evolution is precisely equivalent to that of a potential temperature distribution θ^* on a solid boundary. The latter problem has been analyzed by Blumen (1978) and Hoyer and Sadourney (1982). The main results are that the nonlinear cascade to small scales is governed by a $k^{-8/3}$ energy spectrum and that the Rossby number increases as $k^{2/3}$. The application of the theory to the tropopause, with the finite static stability of the stratosphere taken fully into account, provides an important new view of nonlinear atmospheric dynamics. The tropopause is less influenced by frictional effects than air immediately above the ground, implying that scaling arguments based on inviscid nonlinear dynamics will have greater relevance. With this in mind, the derivation of the spectral slopes for "θ turbulence" is summarized below.

The derivation below uses only dimensional analysis. This approach emphasizes that these results depend only on the assumption that nonlinear interactions are local in wavenumber space and that they do not depend on any of the additional assumptions and approximations that go into the closure theories used by the authors cited above.

There are two global conserved quantities that constrain the nonlinear dynamics: the energy, $E = \int [\frac{1}{2}(u^2 + v^2) + \frac{1}{2}(g\theta'/N\theta_0)^2]dV$, and the variance of the potential temperature on the tropopause, $\Theta = \int \theta_{tp}'^2 dA$. The latter is conserved as a consequence of the material conservation of potential temperature following trajectories on the tropopause and the nondivergence of the geostrophic velocity field. These global constants are related to the Fourier coefficients of the streamfunction through the results of section 3 as follows:

$$E = \int_0^\infty E(k)dk,$$

$$E(k) = f\left(\frac{1}{N_t} + \frac{1}{N_s}\right)k^2 \int_0^{2\pi} |\psi(\mathbf{k})|^2 d\phi, \qquad (7.1)$$

$$\Theta = \int_0^\infty \Theta(k)dk,$$

$$\Theta(k) = \left(\frac{\theta_{00}N_sN_t}{g(N_s - N_t)}\right)^2 k^3 \int_0^{2\pi} |\psi(\mathbf{k})|^2 d\phi, \qquad (7.2)$$

where ϕ is the orientation of the horizontal wave vector $\mathbf{k}$. The energy is partitioned between the troposphere and stratosphere in proportion to the inverse of the Brunt–Väisälä frequency—that is, with more energy in the troposphere. The energy is equipartitioned between kinetic and potential.

The first step is to determine which constraint dominates in an inertial range. Fjørtoft's (1953) theorem shows that in two-dimensional vortex dynamics the cascade to small scales is controlled by the conservation of enstrophy, while that to large scales is controlled by conservation of energy. Similar results are obtained by the same method below.

If variance initially concentrated at wavenumber k_0 is transferred to k_1 and k_2, then conservation of Θ and E, respectively, implies

$$\Theta(k_1) + \Theta(k_2) = \Theta(k_0) \qquad (7.3)$$

and

$$\frac{\Theta(k_1)}{k_1} + \frac{\Theta(k_2)}{k_2} = \frac{\Theta(k_0)}{k_0}. \qquad (7.4)$$

Eliminating $\Theta(k_0)$ gives

$$\frac{k_1 - k_0}{k_1}\Theta(k_1) + \frac{k_2 - k_0}{k_2}\Theta(k_2) = 0. \qquad (7.5)$$

Similar equations are given by Blumen (1978) for the more general flow including two solid boundaries. The results given here correspond to Blumen's when the limit $kH \to \infty$ is taken in the latter, where H is the vertical separation of the two boundaries. From Eq. (7.5) it can be deduced that either $k_1 < k_0 < k_2$ or $k_2 < k_0 < k_1$. In other words, the variance must be divided between one wavenumber greater than k_0 and another less than k_0. The evolution of the energy or temperature variance spectra can be illustrated by the respective mean wavenumbers,

$$\langle k \rangle_E = \frac{\int kE(k)dk}{\int E(k)dk} = k_0, \qquad (7.6)$$

$$\langle k\rangle_\Theta = \frac{\int k\Theta(k)dk}{\int \Theta(k)dk} = \frac{k_0^2 + (k_2 - k_0)(k_0 - k_1)}{k_0} > k_0. \tag{7.7}$$

Similarly, weighted means of $\ln k$ can be calculated, giving

$$\langle \ln k\rangle_E < \ln k_0, \tag{7.8}$$

$$\langle \ln k\rangle_\Theta > \ln k_0. \tag{7.9}$$

These relations imply that spreading of variance in wavenumber space is accompanied by a general transfer of energy to large scales and temperature variance to small scales. It is worth noting, however, that although $\langle \ln k\rangle_E$ decreases $\langle k\rangle_E$ remains constant, implying that the energy transfer is relatively weak.

The scaling laws that govern the energy and temperature variance cascades can be derived using dimensional analysis. This technique has been applied to a general class of two-dimensional equations, including both vortex dynamics and potential temperature dynamics, by Pierrehumbert et al. (1994). Under the assumption that eddy interactions are localized in wavenumber space the timescale of the interactions must be related to the local vorticity, giving

$$\tau(k) \approx (k^3\Theta(k))^{-1/2}. \tag{7.10}$$

This timescale is based on vorticity values at the tropopause, which scale as $k^3E(k)$, as opposed to the three-dimensional vorticity distribution, which scales as $k^2E(k)$. On this timescale it is assumed that the relevant conserved quantity is moved a fixed distance in $\ln k$, so that the flux of, for instance, temperature variance is given by

$$F_\Theta = \frac{k\Theta(k)}{\tau(k)}. \tag{7.11}$$

For a steady cascade the flux F_Θ must be independent of k. Using Eq. (7.10) for τ then gives

$$\Theta(k) \propto k^{-5/3}, \quad E(k) \propto k^{-8/3}, \tag{7.12}$$

for the cascade to small scales. Similarly the scaling law for the energy cascade is determined by setting $F_E = kE\tau^{-1} = \text{const}$, giving

$$\Theta(k) \propto k^{-1}, \quad E(k) \propto k^{-2}. \tag{7.13}$$

For the downscale cascade the slope is only slightly different from the k^{-3} deduced by Charney. The $-8/3$ slope has also been predicted by Andrews and Hoskins (1978), based on a semigeostrophic model of frontal collapse. There does not appear to be any direct relationship between the latter model, which was time dependent and semigeostrophic, and the current quasigeostrophic prediction. There are, however, some interesting parallels. In both cases enstrophy is cascaded to infinite wavenumber in a finite time. In the present case this can be seen by combining (7.10) and (7.12) to give

$$\tau(k) \propto k^{-2/3}. \tag{7.14}$$

The decrease in τ with increasing wavenumber leads to an ever accelerating transfer to smaller scales. The increasing intensity at small scales justifies the assumption made above that interactions are local, since the small scales are predicted to evolve too rapidly to be affected by large-scale motions. This is in marked contrast to the Charney theory, which predicts a constant τ. With a constant timescale the assumption of local interactions cannot be fully justified. In numerical simulations of two-dimensional barotropic turbulence, which is closely analogous to the three-dimensional quasigeostrophic turbulence studied by Charney, it has been found that the nonlocal interactions prevent the predicted k^{-3} inertial cascade from emerging (e.g., Legras et al. 1988). The wavenumber dependence of Rossby number at the tropopause might provide a means of distinguishing between this theory and that of Charney (1971) in observed data. Associated with the decrease in τ there is an increase in Rossby number as k increases, so that at some stage the quasigeostrophic approximation must break down.

The relative strength of the tropopause anomalies compared with internal troposphere anomalies, as displayed in Figs. 1 and 2, suggest that Blumen's theory is of more relevance to tropospheric dynamics than Charney's. The implication is that the large-scale flow has a greater role in driving ageostrophic small-scale motion than implied by the latter theory. The scaling arguments given above, however, only hint at the possibilities: further research is required to gain a true understanding of the nature of this cascade to small scales.

8. Discussion

The dynamics of the tropopause has been analyzed with the idealization of uniform potential vorticity in the troposphere and stratosphere. Elementary quasigeostrophic theory yields a simple local relation between the height and potential temperature of the tropopause. This relation provides an important link between two fundamental dynamical properties. It is interesting that, compared with the elliptical operator relevant to three-dimensional PV anomalies, the inversion operator here takes such a simple form.

There are two caveats to be made. First, on the large scale, the f-plane approximation is suspect. This reservation applies particularly to section 6, where it is shown that, insofar as the f-plane approximation provides a qualitative model of midlatitude synoptic dynamics, the tendency of baroclinic eddies to homogenize potential vorticity within the troposphere leads to a constraint on the structure of the zonal-mean jet. The details of this constraint will certainly be affected by spherical geometry, variation in the Coriolis parameter,

and ageostrophic terms. Nevertheless, the large-scale flow is balanced and as such should be determined from the potential vorticity through an inversion operation (Hoskins et al. 1985). So long as this inversion operator retains the elliptical nature of the quasigeostrophic inversion the number of boundary conditions that can be imposed will remain the same. If this is true a constraint of the nature discussed in section 6 might apply to more realistic flow. Some evidence of such a constraint has been found in calculations using the full Ertel's potential vorticity and spherical geometry (Sun and Lindzen 1994).

The second caveat concerns the smaller scales. On these scales much interest in the dynamics of the tropopause is focused on tropopause folding. The quasigeostrophic dynamics discussed here is not directly relevant to such events, since ageostrophic effects must become important.

The large-scale atmospheric flow is often treated as being barotropic, or equivalent barotropic. Energy converted to kinetic energy by baroclinic instability is transferred by nonlinear dynamics to barotropic modes (e.g., Hoyer and Sadourny 1982; Hoskins et al. 1985). The structures discussed in this paper are, strictly speaking, baroclinic, being associated with strong temperature anomalies. Within the formulation of the Eady model, for instance, there is no possibility of barotropic flow, as all the dynamics is contained in temperature anomalies. However, when the temperature anomalies of the tropopause and ground are in phase the flow has a structure usually associated with barotropic flow. For instance, the sign of the vorticity anomaly is independent of depth.

Although potential temperature anomalies on the tropopause and lower boundary can be expressed as potential vorticity anomalies with a δ-function z dependence, the dynamics of those anomalies is fundamentally different from the dynamics of a homogeous PV distribution. Section 7 shows that the cascade of θ variance to small scales leads to increasing Rossby numbers and the eventual breakdown of the quasigeostrophic approximation. The relation between the work of Charney (1971) and that of Blumen (1978), reviewed in section 7, is similar to that between the two well-known classic models of baroclinic instability developed by Charney (1947) and Eady (1949), respectively. The first neglects the tropopause and models the interaction of lower boundary temperature gradient with internal meridional gradients of Ertel's potential vorticity (PV). The second, on the other hand, neglects horizontal gradients of PV and models the interaction of the lower boundary with the tropopause.

Acknowledgments. This work was funded by the British Antarctic Survey, as part of the Second Antarctic Special Topic Program, and the U.K. Universities Global Atmospheric Modelling Project. I have used the UGCM largely as a black box; it is maintained by a large group—the principal contributors to the version used here were M. Blackburn, J. Thuburn, and P. Valdes. I have benefited from helpful discussions with many people, especially C. Bishop, G. Craig, J. Egger, G. Hartjenstein, T. Hewson, B. J. Hoskins, I. N. James, A. Thorpe, and V. Wirth. Helpful reviews were given by I. Held, P. Thompson, and an anonymous referee.

REFERENCES

Andrews, D. G., and B. J. Hoskins, 1978: Energy spectra predicted by semi-geostrophic theories of frontogenesis. *J. Atmos. Sci.*, **35**, 509–512.

Bannon, P. R., 1989: On deep quasi-geostrophic theory. *J. Atmos. Sci.*, **46**, 3457–3463.

Blumen, W., 1978: Uniform potential vorticity flow: Part I. Theory of wave interactions and two-dimensional turbulence. *J. Atmos. Sci.*, **35**, 774–783.

Boer, G. J., and T. G. Shepherd, 1983: Large-scale two-dimensional turbulence in the atmosphere. *J. Atmos. Sci.*, **40**, 164–184.

Bretherton, F. P., 1966: Critical layer instability in baroclinic flows. *Quart. J. Roy. Meteor. Soc.*, **92**, 325–334.

Charney, J. G., 1947: The dynamics of long waves in a baroclinic westerly current. *J. Meteor.*, **4**, 135–162.

——, 1971: Geostrophic turbulence. *J. Atmos. Sci.*, **28**, 1087–1095.

Danielsen, E. F., 1968: Stratospheric–tropospheric exchange based on radioactivity, ozone and potential vorticity. *J. Atmos. Sci.*, **25**, 502–518.

Eady, E. T., 1949: Long waves and cyclone waves. *Tellus*, **1**(3), 33–52.

Farrell, B., 1984: Modal and non-modal baroclinic waves. *J. Atmos. Sci.*, **41**, 668–673.

Fjørtoft, R., 1953: On the changes in the spectral distribution of kinetic energy for two-dimensional, nondivergent flow. *Tellus*, **5**, 225–230.

Garner, S. T., N. Nakamura, and I. M. Held, 1992: Nonlinear equilibration of two-dimensional Eady waves: A new perspective. *J. Atmos. Sci.*, **49**, 1984–1996.

Held, I. M., 1982: On the height of the tropopause and the static stability of the troposphere. *J. Atmos. Sci.*, **39**, 412–417.

Hoskins, B. J., M. E. McIntyre, and A. W. Robertson, 1985: On the use and significance of isentropic potential vorticity maps. *Quart. J. Roy. Meteor. Soc.*, **111**, 877–946 (see also addendum, **113**, 402–404).

Hoyer, J.-M., and R. Sadourny, 1982: Closure modeling of fully developed baroclinic instability. *J. Atmos. Sci.*, **39**, 707–721.

Juckes, M. N., I. N. James, and M. E. Blackburn, 1994: The influence of Antarctica on the momentum budget of the southern extratropics. *Quart. J. Roy. Meteor. Soc.*, **120**, 1017–1044.

Legras, B., P. Santangelo, and R. Benzi, 1988: High-resolution numerical experiments for forced two-dimensional turbulence. *Europhys. Lett.*, **5**, 37–42.

Li, D., 1992: The damping of two-grid waves in the lower stratosphere in the UGAMP GCM by modification of the radiation scheme. UGAMP Tech. Rep. 23, Dept. of Meteorology, University of Reading, Reading, U.K.

Pedlosky, J., 1987: *Geophysical Fluid Dynamics.* Springer-Verlag, 710 pp.

Pierrehumbert, R. T., I. M. Held, and K. Swanson, 1994: Spectra of local and nonlocal two-dimensional turbulence. *Chaos, Solitons and Fractals*, in press.

Reed, R. J., 1955: A study of a characteristic type of upper-level frontogenesis. *J. Meteor.*, **12**, 226–237.

Rivest, C., C. A. Davis, and B. F. Farrell, 1992: Upper-tropospheric synoptic-scale waves. Part I: Maintenance as Eady normal modes. *J. Atmos. Sci.*, **49**, 2108–2119.

Sun, D.-Z., and S. R. Lindzen, 1994: A PV view of the zonal-mean distribution of temperature and wind in the extratropical troposphere. *J. Atmos. Sci.*, **51**, 757–772.